Random Tilings: Concepts and Examples

Christoph Richard, Moritz Höffe, Joachim Hermisson and Michael Baake

Institut für Theoretische Physik, Universität Tübingen, Auf der Morgenstelle 14, D-72076 Tübingen, Germany

January 10, 2000

Abstract

We introduce a concept for random tilings which, comprising the conventional one, is also applicable to tiling ensembles without height representation. In particular, we focus on the random tiling entropy as a function of the tile densities. In this context, and under rather mild assumptions, we prove a generalization of the first random tiling hypothesis which connects the maximum of the entropy with the symmetry of the ensemble. Explicit examples are obtained through the re-interpretation of several exactly solvable models. This also leads to a counterexample to the analogue of the second random tiling hypothesis about the form of the entropy function near its maximum.

1 Introduction

Perfect quasiperiodic tilings provide useful tools for the description of certain thermodynamically stable quasicrystals [26, 32, 49], at least for their averaged structure. However, it is widely accepted that the perfect structure is an idealization, and that a systematic treatment of defectiveness is necessary for all but a few quasicrystals [12, 18, 30]. In particular, starting from the perfect structure, the inclusion of local defects [12] is helpful to overcome a number of pertinent problems, ranging from the observed degree of imperfections [15] to the impossibility of strictly local growth rules for perfect quasiperiodic patterns [50].

An alternative approach relies on a stochastic picture and adds an entropic side to the stabilization mechanism. Its most prominent representatives are usually formulated in terms of so-called random tilings [18, 29, 30]. It has long been argued that such stochastic tilings should provide a more realistic description both of the structures with their intrinsic imperfections and of their stabilization, which is then mainly entropic in nature.

Recently, improved methods have been suggested [34] to test this hypothesis in practice, and the results support the claim that such models are realistic and relevant [35]. Further impetus is given by the very recent progress to grow (almost) equilibrium random tilings on the computer [33] in suitable grand-canonical ensembles.

The concept of entropic stabilization applies to a wide class of – not necessarily quasicrystalline – tiling ensembles (defined through a set of proto-tiles and packing rules). However, within the original approach to random tilings (see [30] for a review), only a (while interesting) rather special subset of these can be described. This is because two concepts are mixed here that, in principle, have nothing to do with each other: the mechanism of entropic stabilization and the concept of the phason strain, the latter being used for the description of quasicrystalline order for those tilings that allow a so-called height representation. Hereby, the phasonic language is used throughout, restricting the range of applicability.

In this paper, we propose a more elementary and, at the same time, more rigorous point of view which directly employs the densities of the tiles to describe the phase diagram. While allowing for adequate generality, the new picture conforms to the other one, if this exists – at least, if the relation between the tile densities and the strain parameters is locally linear.

This reformulation is, however, not done for mere aesthetic reasons, but has a number of advantages and leads to consequences of direct interest. In particular, the generality of the approach now makes classes of exactly solvable models accessible – e. g. examples compatible with *crystallographic* symmetries – which already show a variety of interesting and typical phenomena.

For an explicit result, let us mention the two so-called random tiling hypotheses. The validity of these hypotheses is the usual set-up for an elastic theory in order to show the existence of a diffraction pattern with Bragg peaks for three-dimensional tilings, see [30] and, for a recent discussion of experimental results, [17]. The first hypothesis assumes that the point of maximum entropy in the phase space is one of maximal symmetry. We will show below how it can be derived from more basic assumptions as a consequence, and need not be stated as hypothesis. The second hypothesis uses the phasonic picture of quasicrystals to establish a kind of elastic theory. The hypothesis would now state that the entropy is locally a quadratic function of the densities near its maximal value, and the Hessian can be interpreted as an entropic elasticity tensor. However, this picture should to be taken with a pinch of salt: we shall show a counterexample where the maximum is unique, but coincides with a second order phase transition and is thus *not* of quadratic nature.

In the conventional setup much information, such as elastic constants and diffraction properties, are extracted from the correlations of the height variables. The fundamental variable analogous to the height correlations in our picture turns out to be the *covariance* *matrix* of the tile numbers.

Let us sketch how the paper is organized. The following section is devoted to the introduction of our concept and the thermodynamic formalism used. After a brief discussion of the class of (generalized) polyomino tilings [23], which comprises all our examples, we will illustrate our concepts by simple examples in one dimension. In the section on symmetry versus entropy, we present an argument on how to derive the first random tiling hypothesis from elementary assumptions. This is then substantiated by various planar examples, where our focus is on the re-interpretation of exactly solvable models which thereby gain a slightly different interpretation and, eventually, even another application. Our examples are taken from dimer models, but also the three-colouring model on the square lattice and hard hexagons are discussed.

2 Setup and preliminaries

In this section, we describe the way how we deal with random tilings. Since we do not want to use the special and somewhat restrictive phasonic picture for our fundamental definitions, these will differ from those given elsewhere [30].

As a *(random) tiling* we define a face-to-face space filling with tiles from a finite set of prototiles, without any gaps or overlaps. There might be a number of additional local packing rules specifying the allowed tilings. The number of allowed patches should increase exponentially with the volume of the patch (and hence with the number of tiles), resulting in a positive entropy density for the tiling ensemble, which we then call *random tiling ensemble*. For the tiling ensemble being homogeneous, prototile shapes and packing rules should admit tilings containing all sorts of tiles (with positive density), otherwise the ensemble splits into different subensembles that have to be taken into account separately.

With this setting, random tilings in the sense of [30] are included as a proper subset. In order to give the thermodynamic limit a precise meaning, we formalize the definition as follows.

For a random tiling of the space R^d, its *prototiles* $\mathcal{T}_i$ are compact, connected subsets of R^d of positive volume l_i, homeomorphic to balls. Let $\Lambda \subset R^d$ be given as connected, compact set of positive volume $V(\Lambda)$. We now have to explain our notion of a patch. If P_Λ is a collection of translated prototiles, we call P_Λ a Λ-*patch* iff P_Λ is a covering of Λ (without gaps) such that each element of P_Λ has a nonempty intersection with Λ, and every two elements have empty common interior. We call two Λ-patches *equivalent* iff they are translates of each other. For fixed prototile numbers $n_1, \ldots, n_M$ (with corresponding densities $\rho_i = l_i n_i / V(\Lambda)$), let us denote the number of non-equivalent Λ-patches by $g_\Lambda(n_1, \ldots, n_M)$.

It should be stressed here that, in principle, we can impose any type of boundary conditions for our definitions. However, *free boundary conditions* are the natural ones to choose from a physical point of view – a different choice may indeed lead to deviating results; fixed boundary conditions in particular seem to be too restrictive in most cases

[54, 19, 43]. On the other hand, most of the exact results have been obtained by use of periodic boundary conditions, and it has to be shown, for each example, that the results also apply to the case of free boundary conditions.

We will use a grand-canonical formulation in the following, in difference to the (usual) canonical treatment of tiling ensembles [30, 44], as we believe that an ensemble with fluctuating tile numbers is the adequate setup to cover processes such as local rearrangements or tiling growth. Moreover, this formulation will prove advantageous for our arguments and practical calculations.

As we are interested in configurational entropy only, we will assign equal (zero) energy to every prototile. In this situation, the chemical potentials of the prototiles are the only parameters remaining. As variables conjugated to the densities, we introduce chemical potentials μ_i as well as activities $z_i = e^{\mu_i}$ for every prototile, [1] $(i = 1, \ldots, M)$, and define the grand-canonical partition function to be the configuration generating function

$$\mathcal{Z}_\Lambda(\mu_1, \ldots, \mu_M) = \sum_{n_1, \cdots, n_M} g_\Lambda(n_1, \ldots, n_M) z_1^{\ell_1 n_1} \cdots z_M^{\ell_M n_M}. \tag{1}$$

Since we are interested in the entropic behaviour of large systems, we define the grand-canonical potential [2] per unit volume to be the limit

$$\phi(\mu_1, \ldots, \mu_M) = \lim_{\Lambda \to \infty} \frac{1}{V(\Lambda)} \log \mathcal{Z}_\Lambda(\mu_1, \ldots, \mu_M). \tag{2}$$

Here, $\{\Lambda\}$ is any collection of connected, compact subsets of R^d of positive volume $V(\Lambda)$ such that $\lim V(\Lambda) = \infty$ and $\lim B(\Lambda)/V(\Lambda) = 0$, where $B(\Lambda)$ denotes (the maximum) over the *volume of the boundary tiles* of any Λ-patch, in the same spirit as the van Hove limit taken for ensembles in statistical mechanics [55]. For models of physical relevance the thermodynamic limit defined that way should exist for all physical quantities and be independent of the special choice of the limit sequence $\{\Lambda\}$.

The mean (volume) densities of the different prototiles in this ensemble can be computed as

$$\bar{\rho}_i(\mu_1, \ldots, \mu_M) = \lim_{\Lambda \to \infty} \frac{1}{V(\Lambda)} \langle l_i n_i \rangle_\Lambda = \frac{\partial \phi(\mu_1, \ldots, \mu_M)}{\partial \mu_i} \quad (i = 1, \ldots, M), \tag{3}$$

where $\langle\ \rangle_\Lambda$ denotes the finite-size ensemble average for given chemical potentials $\mu_1, \ldots, \mu_M$.

Note that all physical quantities defined here are *ensemble averages*. In cases where these quantities differ from corresponding values of a *typical* representative of the ensemble, one has to reflect whether the grand-canonical setup fits the experimental situation, or if a canonical ensemble is the correct choice. Bear in mind, however, that the van Hove

[1] We suppress extra prefactors β in all definitions below.

[2] If Boltzmann-factors are taken instead of activities, this corresponds to the (canonical) free energy in statistical mechanics.

limit is not properly defined for single tilings that are not self-averaging. Thus either canonical and grand-canonical thermodynamics coincide, or the the canonical picture is likely not to be well defined at all.

So far, the chemical potentials and also the conjugated (mean) densities do not form an *independent* set of macroscopical parameters to describe the ensemble. We always have $\sum_{i=1}^{M} \bar{\rho}_i = 1$ as normalization constraint, and in general, the tile geometries and packing rules may eventually impose further constraints on the densities.

In order to make the notion of macroscopical independence precise, let $v = \sum v_j n_j \neq 0$ be an arbitrary linear combination of some prototile numbers n_j, with real coefficients v_j. We call the accompanying set of tile densities $\{\bar{\rho}_j\}$ *independent* in the thermodynamic limit, iff the variance per unit volume of v is strictly positive for any choice of the v_j:

$$\langle\langle v \rangle\rangle := \lim_{\Lambda\to\infty} \frac{1}{V(\Lambda)} \langle (v - \langle v \rangle_\Lambda)^2 \rangle_\Lambda \quad > \; 0. \tag{4}$$

The *degrees of freedom* of the tiling ensemble are given by a maximal set of independent densities. One checks that, with this definition, normalization reduces the independent densities by one, and there is no additional freedom due to surface effects or subclasses of the ensemble that do not contribute entropically.

In general, since the average taken in (4) depends on the chemical potentials, the variance of some v may vanish only for a special choice of the potentials leading to a reduction of independent densities at isolated points of the phase space. However, no such thing will happen in any of the examples we discuss in this sequel and, for simplicity of the presentation, we exclude this possibility in the following.

Let us mention a consequence of this definition for the covariance matrix of the tile numbers (which corresponds to the isothermal compressibility in the thermodynamic situation), in the thermodynamic limit:

$$\kappa_{ij} = \lim_{\Lambda\to\infty} \frac{1}{V(\Lambda)} \Big(\langle l_i n_i l_j n_j \rangle_\Lambda - \langle l_i n_i \rangle_\Lambda \langle l_j n_j \rangle_\Lambda \Big) = \frac{\partial \bar{\rho}_i}{\partial \mu_j} \qquad (i,j = 1,\dots,M). \tag{5}$$

This matrix describes tile fluctuations around the mean density and correlations among different tiles. A straightforward calculation shows that (5) is indeed strictly positive iff it is restricted to the subspace of density parameters that had been chosen independently according to the above definition.

In general, a linear constraint on the tile numbers of the form

$$\sum_{j=1}^{M} v_j (l_j n_j) = cV(\Lambda) + \mathcal{O}(V^\alpha(\Lambda)) \qquad (\alpha < 1,\; c \in R) \tag{6}$$

leads to linear variation of the grand-canonical potential in certain coordinate directions:

$$\phi(\mu_1 + v_1 t, \dots, \mu_M + v_M t) = \phi(\mu_1, \dots, \mu_M) + ct \qquad (t \in R). \tag{7}$$

For each constraint of this form, we can shift a single chemical potential to zero in the grand-canonical potential by a suitable choice of t.

Let us choose an independent subset of macroscopic parameters, $\bar{\rho}_1, \ldots, \bar{\rho}_k$ say, which we abbreviate as $\{\bar{\rho}\}$, and write the random tiling entropy as a function of these independent densities. According to the considerations above, this can be done as follows. We set $\mu_{k+1} = \cdots = \mu_M = 0$ in (1), i.e. we normalize the grand-canonical potential by an appropriate choice of the origin of the energy scale. We call the normalized grand-canonical potential ϕ again. From (7) and (3) it is readily verified that the normalization of ϕ leaves the independent densities invariant.

The (grand-canonical) entropy per unit volume as a function of the independent (mean) tile densities is obtained as Legendre transform of the (normalized) grand-canonical potential [3] with respect to the conjugated chemical potentials,

$$s(\bar{\rho}_1, \ldots, \bar{\rho}_k) = \phi(\mu_1(\{\bar{\rho}\}), \ldots, \mu_k(\{\bar{\rho}\})) - \sum_{i=1}^{k} \bar{\rho}_i \mu_i(\{\bar{\rho}\}). \tag{8}$$

Note that the Legendre transform is well defined owing to the non-singularity of the matrix

$$\frac{\partial^2 \phi(\mu_1, \ldots, \mu_k)}{\partial \mu_i \partial \mu_j} = \kappa_{ij} \qquad (i, j = 1, \ldots, k). \tag{9}$$

Let us locate the maximum of the entropy curve as a function of the independent densities $\bar{\rho}_1, \ldots, \bar{\rho}_k$. We have by definition

$$\frac{\partial s(\{\bar{\rho}\})}{\partial \bar{\rho}_j} = -\mu_j(\{\bar{\rho}\}) \quad (j = 1, \ldots, k). \tag{10}$$

It follows that the entropy is extremal, $s_{\max} = \phi$, at $\mu_1 = \cdots = \mu_k = 0$. (For the grand-canonical potential (2) this point occurs at $\mu_1 = \cdots = \mu_M = 0$.) This is the situation of the maximal random ensemble where each configuration is weighted equally. Let us take a closer look at the Hessian, the matrix of the second derivative

$$\frac{\partial^2 s(\{\bar{\rho}\})}{\partial \bar{\rho}_i \partial \bar{\rho}_j} = -\frac{\partial \mu_j(\{\bar{\rho}\})}{\partial \bar{\rho}_i} = -\left(\kappa^{-1}\right)_{ij} \qquad (i, j = 1, \ldots, k). \tag{11}$$

If s is locally C^3, we conclude that the entropy is a concave function everywhere. On the other hand, also in the vector space of the independent densities, the variance of v and hence the covariance matrix (5) may diverge in the thermodynamic limit for certain values of the chemical potentials. This generally occurs at phase transitions. In this case the Hessian of the entropy has 0 as an eigenvalue in the large system limit; we will give an example below where this happens at the point of maximum entropy. For all other

[3] Under the above assumption, this definition coincides with the micro-canonical one [51]; for a number of examples in the sequel this can be shown explicitly.

situations, the shape of the entropy curve near its maximum is completely determined by the Hessian.

We interpret the negative of the Hessian, at the point of maximum entropy, as tensor of *entropic elasticity*. Without any further symmetry, we refer to its eigenvalues as the *elastic constants* of the random tiling ensemble. We will define a symmetry-adapted version in the section on symmetry.

3 Polyomino tiling ensembles

A class of (crystallographic) tilings that allow a re-interpretation of many exactly solved models are the (generalized) polyomino tilings, see [23, 43] for definitions and background material. Their prototiles are taken from one or combinations of several elementary cells of a given periodic graph. There may be as well certain packing rules, resulting in restricted random tiling ensembles. We will give a number of examples of tilings consisting of monominoes and dominoes.

The simplest class of random tilings are tilings of (coloured) monominoes without further restrictions. For lattices of any dimension, this results in Bernoulli ensembles [53]. A natural way to impose packing rules for these models is to exclude the occurrence of clusters with moniminoes of the same colour. For nearest-neighbour exclusion on lattices, the restriction is hierarchical: the tiling can be regarded as being built from consecutive layers of "hypertilings" with additional constraints along the layer direction. In this case, the entropy is bounded by the entropy of the corresponding hypertiling ensemble. Several two-dimensional examples are discussed below.

We should mention the one-to-one correspondence between polyomino tilings on a periodic graph Λ and polymer arrangements on the dual cell complex Λ^* (the so-called Delone complex). This is illustrated in figure 1 for a simple case, the monomer-dimer system on the square lattice.

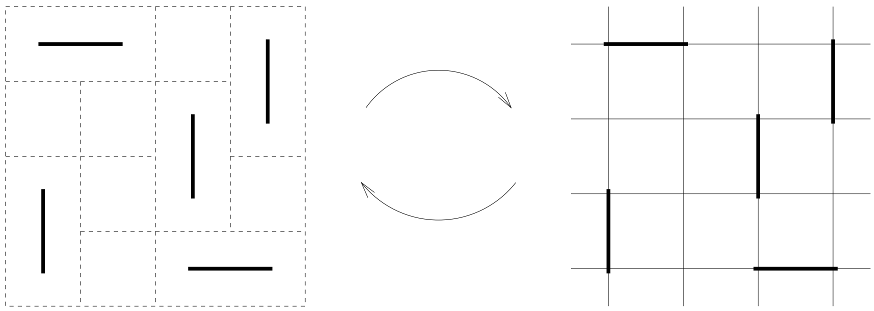

Figure 1: Each polyomino tiling is a polymer configuration on the dual cell complex.

Owing to this connection, the (pure) domino problem can be solved in a number of cases in two dimensions, as the dual fully packed dimer problem allows the exact solution on planar graphs by means of Pfaffians [4]. This has been shown by Kasteleyn in [38, 39], where he computed the entropy of dimers on the square lattice. It is even possible to compute densities of finite patches explicitely, which has recently been shown by Kenyon [40]. We will treat two examples representing the different types of critical behaviour of the solvable domino systems [48]: systems of Onsager type (with logarithmic singularity of the covariance matrix) and systems of Kasteleyn type (with square-root singularity of the covariance matrix).

Let us consider monomino-domino tilings without restriction next. The one-dimensional system will be discussed below. In two dimensions, there are various connections with other models, e. g. for the triangle-rhombus tiling on the triangular lattice [59], but, to our knowledge, no explicit exact solutions. On the other hand, as follows from the theory of monomer-dimer systems [28], phase transitions can only occur for tilings with *vanishing* monomino density, regardless of the dimensionality of the system – these phases are the (pure) domino tilings mentioned above. There is at least one monomino-domino tiling with constraints that allows for exact solution in two dimensions: the tiling on the hexagonal lattice together with exclusion of neighbouring dominoes on different sublattices. This tiling ensemble is equivalent to the ensemble of hard hexagons [9, 11], see also below.

4 Unrestricted and one-dimensional examples

The simplest class of random tilings, built from M coloured monominoes on an arbitrary lattice, can be described purely combinatorially. There are no local constraints or packing rules, and thus no global constraints for the densities besides normalization. One application of this model is the description of unrestricted chemical disorder in multicomponent alloys [6].

The thermodynamic limit may be taken by counting the number of monomino configurations on consecutive lines of length N. In this simple case, the densities ρ_i [5] can be given as explicit expressions of the activities:

$$\rho_i = \frac{z_i}{z_1 + \ldots + z_M} \qquad (i = 1, \ldots, M). \tag{12}$$

In order to eliminate the normalization constraint, we choose $\rho_1, \ldots, \rho_{M-1}$ as independent densities and normalize the grand-canonical potential via

$$\tilde{\phi}(\mu_1, \ldots, \mu_{M-1}) := \phi(\mu_1, \ldots, \mu_{M-1}, 0). \tag{13}$$

Both functions are related via (7),

$$\tilde{\phi}(\mu_1 - \mu_M, \ldots, \mu_{M-1} - \mu_M) = \phi(\mu_1, \ldots, \mu_M) - \mu_M. \tag{14}$$

[4] For an introduction into the Pfaffian method, we refer to Appendix E of [57].
[5] We suppress the overbar and write ρ_i instead of $\bar{\rho}_i$ from now on.

We obtain the entropy as Legendre transform of the normalized grand-canonical potential,

$$s(\rho_1,\dots,\rho_{M-1}) = -\sum_{j=1}^{M} \rho_j \log \rho_j, \tag{15}$$

where $\rho_M = 1-\sum_{j=1}^{M-1}\rho_j$. This coincides with the entropy of a Bernoulli system [53] with fixed frequencies $p_i = \rho_i$. The entropy function is strictly concave and takes its (unique) maximum at the point $\rho_1 = \dots = \rho_M = \frac{1}{M}$, with value

$$s_{\max} = -\sum_{j=1}^{M} \frac{1}{M}\log\frac{1}{M} = \log M. \tag{16}$$

Near its maximum, the entropy curve is a quadratic function of the independent order parameters. Its shape near this point is completely determined by the Hessian

$$\left.\frac{\partial^2 s}{\partial\rho_i\partial\rho_j}\right|_{s=s_{\max}} = -\left.\left(\rho_M^{-1}+\rho_i^{-1}\delta_{ij}\right)\right|_{s=s_{\max}} = -M(1+\delta_{ij}) \qquad (i,j=1,\dots,M-1). \tag{17}$$

The negative Hessian is the elastic tensor. In particular, for $M=2$, we obtain

$$s(\rho) = \log 2 - 2\left(\rho-\frac{1}{2}\right)^2 + \mathcal{O}\left(\left(\rho-\frac{1}{2}\right)^4\right) \tag{18}$$

which (with $E = 2\rho - 1$) conforms to the phasonic expression given in [30].

Owing to the lack of geometric or other constraints, this class of examples is fully controlled by the strong law of large numbers [7]: With probability one, for a given member of the ensemble, the probability to occupy a position with a tile of type j is its frequency, p_j. This even connects the growth with the equilibrium properties, as also observed recently for other, more complicated ensembles [33].

A first natural step to examine the effect of different tile geometries as well as of certain packing rules is to allow these in one coordinate direction. Introducing different tile sizes, one of the simplest models is the 1D monomino-domino model [28].

Similar to the previous example, the only constraint of this model is due to density normalization. We eliminate this constraint in the same way, i.e. we write

$$\mathcal{Z}_N(\mu) = \sum_{k=0}^{N} g_N(k) z^k \tag{19}$$

where $g_N(k)$ is the number of connected patches with N occupied sites, k of which being monominoes. So, $\mu = \log z$ is the chemical potential of a monomino. Obviously, $\mathcal{Z}_N(\mu)$ fulfils the Fibonacci-type recursion formula

$$\mathcal{Z}_N(\mu) = z\mathcal{Z}_{N-1}(\mu) + \mathcal{Z}_{N-2}(\mu) \tag{20}$$

$$\mathcal{Z}_0 := 1 \qquad \mathcal{Z}_1(\mu) = z.$$

The quotient $\mathcal{Z}_N(\mu)/\mathcal{Z}_{N-1}(\mu)$ is a rational function whose limit, for $N \to \infty$, exists and can easily be calculated from (20) to be

$$\lim_{N\to\infty} \frac{\mathcal{Z}_N(\mu)}{\mathcal{Z}_{N-1}(\mu)} = \left(\frac{z}{2} + \sqrt{1+\left(\frac{z}{2}\right)^2}\right). \tag{21}$$

The grand-canonical potential per site is defined through $\phi(\mu) = \lim_{N\to\infty} \frac{1}{N} \log \mathcal{Z}_N(\mu)$, but can directly be calculated from the quotient (21) as

$$\phi(\mu) = \lim_{N\to\infty} \log \frac{\mathcal{Z}_N(\mu)}{\mathcal{Z}_{N-1}(\mu)} = \operatorname{arsinh}\frac{z}{2}. \tag{22}$$

We denote the monomino density by ρ_1, the domino density by ρ_2 ($\rho_1 + \rho_2 = 1$). Let us now write the entropy curve as a function of the monomino density ρ_1. The entropy curve can be computed from the grand-canonical potential as

$$\begin{aligned} s(\rho_1) &= \phi(z(\rho_1)) - \rho_1 \log z(\rho_1) \\ &= (\rho_1 + \frac{\rho_2}{2}) \log(\rho_1 + \frac{\rho_2}{2}) - \rho_1 \log \rho_1 - \frac{\rho_2}{2} \log \frac{\rho_2}{2}, \end{aligned} \tag{23}$$

where

$$\rho_1(\mu) = \frac{\partial \phi(\mu)}{\partial \mu} = \tanh \phi(\mu) = \frac{\frac{z}{2}}{\sqrt{1+\left(\frac{z}{2}\right)^2}}.$$

The entropy function is a strictly concave function with a quadratic maximum

$$s_{\max} = \log \tau \approx 0.4812 \tag{24}$$

at $\frac{2\rho_1}{\rho_2} = \tau \approx 1.6180$, where $\tau = \frac{1+\sqrt{5}}{2}$ denotes the *golden number* [6]. We obtain an elastic constant $\lambda = \frac{5}{4}\sqrt{5} \approx 2.7951$.

It is possible to derive a closed expression for the grand-canonical partition sum [28]. Defining $P_N(x) = i^{-N}\mathcal{Z}_N(2ix)$ transforms the recursion (20) into that of the Chebyshev polynomials of the second kind [1] which are

$$P_N(\cos\theta) = \frac{\sin(N+1)\theta}{\sin\theta} \tag{25}$$

wherefrom one gets

$$\mathcal{Z}_N(\mu) = \frac{1}{\sqrt{1+\left(\frac{z}{2}\right)^2}} \left\{ \begin{array}{c} \cosh \\ \sinh \end{array} \right\} \left((N+1)\operatorname{arsinh}\frac{z}{2}\right), \quad \text{for } N \left\{ \begin{array}{c} \text{even} \\ \text{odd} \end{array} \right\}. \tag{26}$$

[6] The *silver number* $\lambda = 1+\sqrt{2}$ appears in the monomino-domino model of monominoes with two different colours.

Packing rules and supertiles

So far, no further constraint or packing rule has been imposed on the ensembles. A natural way to do this in one dimension is to exclude certain strings of consecuting tiles. In many cases, these ensembles can be directly dealt with by recursive methods as shown above (e.g. the M-colouring problem in 1D), or the constraints can be eliminated by a reformulation of the problem in terms of 'supertiles'. Let us illustrate this for the ensemble of chains in two monominoes a, b with the exclusion of r consecuting a's and s consecuting b's. A moments reflection shows that any allowed chain can (up to boundary tiles) uniquely be written in supertiles $A_{i,j}$, $1 \leq i < r$, $1 \leq j < s$, forming strings of i consecuting a's, followed by j b's. Vice versa, any sequence in the supertiles translates to an allowed one in a, b.

Similarly, the ensemble of monomino chains with tiles a, b and exclusion of bb is equivalent to the monomino-domino model mentioned above. We give the entropy for this ensemble via its 'supertile' formulation with polyominoes $A = a$ and $B = ab$, starting from a Bernoulli ensemble rather than taking different tile geometries of the supertiles into account. The frequencies of the two models are related according to

$$p_a = \frac{p_A + p_B}{p_A + 2p_B}, \qquad p_b = \frac{p_B}{p_A + 2p_B}, \tag{27}$$
$$p_A = 1 - \frac{p_b}{p_a}, \qquad p_B = \frac{p_b}{p_a}.$$

It is obvious from here that the possible values of p_a, p_b are restricted to

$$\frac{1}{2} \leq p_a, \qquad 0 \leq p_b \leq p_a \leq 1. \tag{28}$$

As the entropy per supertile is given by

$$\tilde{s}(p_A, p_B) = -p_A \log p_A - p_B \log p_B, \tag{29}$$

the entropy per (small) monomino follows as

$$\begin{aligned} s(p_a, p_b) &= \left(1 + \frac{p_b}{p_a}\right)^{-1} \tilde{s}(p_A(p_a, p_b), p_B(p_a, p_b)) \\ &= p_a \log p_a - p_b \log p_b - (p_a - p_b) \log(p_a - p_b). \end{aligned} \tag{30}$$

Taking $x = 2p_a - 1$ as parameter, $0 \leq x \leq 1$, the entropy curve is exactly the curve of the monomino-domino model. The maximum occurs at $p_a = \frac{2+\tau}{5} \approx 0.7326$. We obtain an elastic constant $\lambda = 5\sqrt{5} \approx 11.1803$.

However, already in 1D, more complex examples may be considered. An interesting family is provided by the ensemble of square-free words in n letters, $n \geq 3$, which is known to display positive entropy. In fact, the value

$$\tilde{s}(n) = \operatorname{arcosh}\left(\frac{n-1}{2}\right) \tag{31}$$

gives (for $n \geq 4$) a reasonable lower bound of it, which is asymptotically exact, but the determination of the exact value is still an open problem [2].

5 Entropy and symmetry

In this section we consider effects of the symmetries of a tiling ensemble on its entropy function. It should be stressed again that the results below are derived using the grand-canonical formalism. All physical quantities are averages over the whole tiling ensemble. In most situations of physical relevance, however, the ensemble averages coincide with the corresponding quantities of a typical single tiling, and all results translate to the canonical ensemble as well. This will be the case for all examples discussed in this article.

As a symmetry of a random tiling ensemble, we define every linear bijection S_ρ on the density parameters that leaves the entropy function invariant. We write

$$S_\rho : \rho_i \mapsto \tilde{\rho}_i = \sum_{j=1}^{M} S_{ij}\rho_j \qquad (i = 1, \ldots, M). \tag{32}$$

Owing to the normalization constraint, the restriction of S_ρ to the subspace of *independent* density parameters where the entropy function is defined leads in general to an *affine* bijection.

Examples are obtained from bijections on the tiling ensemble which transform densities like (32). They are symmetries of the random tiling ensemble if they respect the thermodynamic limit, i.e. if they induce a bijection on the set of Λ-patches, for each Λ of a suitably chosen limit sequence $\{\Lambda\}$. The simplest examples are colour symmetries, which permute equal prototiles of different colour. Moreover, rotations and reflections on the tiling ensemble, together with a limit sequence of circular sets, lead to *geometric* symmetries. Let us denote every symmetry which is not of the former type as *hidden* symmetry. We will discuss a random tiling with a hidden symmetry below.

In general, every linear bijection on the densities can as well be represented in the vector space of all chemical potentials; as can be verified from (3), a transformation S_ρ induces the adjoint mapping

$$S_\mu : \mu_i \mapsto \tilde{\mu}_i = \sum_{j=1}^{M} (S^*)_{ij}\, \mu_j \qquad (i = 1, \ldots, M), \tag{33}$$

where $S^* = (S^{-1})^t$ means the matrix inverse and transpose of S. In particular, the invariance of the grand-canonical potential under symmetry operations (33) imposes symmetries of the (mean) density vector field in the space of chemical potentials,

$$\tilde{\rho}(\mu) = \rho(\tilde{\mu}). \tag{34}$$

We conclude immediately that symmetry related tiles having equal chemical potential occur with the *same* (mean) density. Note that the point of maximum entropy ($\mu = 0$) is a *fixed point* under any given symmetry which means that symmetries constrain possible density parameters at the entropy maximum. This is precisely the statement of the so-called first random tiling hypothesis:

- The point of maximum entropy is a point of maximum symmetry.

For random tilings with a height representation, maximum symmetry implies zero phason strain, $E \equiv 0$ [30], so this is contained. In our setting, the conlusion above implies:

- At the point of maximum entropy, symmetry related tiles occur with equal (mean) density.

We can further conclude, as can be read off from (34), the density vector ρ, at the point of maximum entropy, has only components in direction of the trivial one-dimensional representations of the symmetry group. Thus, the symmetry determines the entropy maximum completely, if the representation of the symmetry group on the vector space of *independent* density parameters is irreducible (and nontrivial). We will give examples of that kind later on.

Let us now focus on the transformation behaviour of the entropy function (8). This is done most easily within a symmetry-adapted parametrization. By an affine coordinate transformation, it is always possible to introduce new independent density parameters such that the new origin is the point of maximum entropy, and the symmetries are represented by linear, orthogonal transformations. In many cases, the new density parameters have a geometric interpretation in form of densities of supertiles. Let us call these new parameters r and assume that we are in such a frame.

The entropy is invariant under symmetry transformations,

$$s(r) = s(\tilde{r}). \tag{35}$$

At its maximum, the entropy expansion can be written in terms of invariants of the given symmetry group [7]. The form of the second order terms is determined by the Hessian H of the entropy (the matrix of its second derivatives). The symmetries induce a transformation behaviour of the form

$$H|_r = (S_r)^t \, H|_{\tilde{r}} \, S_r. \tag{36}$$

Since S_r is an orthogonal transformation, it *commutes* with H at the point of maximum entropy,

$$H|_o \, S_r = S_r \, H|_o \,. \tag{37}$$

According to Schur's lemma [27], $H|_o$ acts trivially on the irreducible subspaces of the symmetry group and can thus be written as a linear combination of projectors $P^{(i)}$ onto the irreducible components,

$$H|_o = -\sum \lambda_i P^{(i)}. \tag{38}$$

[7] For the *quasicrystal* entropy as a function of perp strain, this kind of arguing was used in [47].

We refer to the λ_i as *elastic constants* of the given random tiling. This is more appropriate than the use of the eigenvalues since they are no longer independent in the presence of symmetries. The quadratic term of the entropy expansion is then of the form

$$s_2(r,r) = -\frac{1}{2}\sum \lambda_i I^{(i)}(r,r), \tag{39}$$

where the $I^{(i)}(r,r)$ are the quadratic invariants defined by

$$I^{(i)}(r,r) = \quad < r, P^{(i)} r >, \tag{40}$$

and $< \cdot,\cdot >$ denotes the scalar product. We will give examples later on.

Now, the discussion on the relation of entropy and symmetry can be extended even further. Above, we have always taken a set of tiles as basic elements to construct the tiling. This is, however, not the only possibility. Instead, tilings can also be seen as built from bonds, vertex configurations, patches of a given volume or number of tiles, or the like. Adopting this point of view, we can assign chemical potentials and densities to patches or bonds rather than to the prototiles. While the number of basic elements and packing rules may increase quite rapidly this way, the above arguments can nevertheless be repeated without change, and we conclude that ensemble densities of symmetry related patches *of any size* are equal at the point of maximum entropy. If the density parameters of a typical tiling of the ensemble coincide with their ensemble averages, then:

- Entropically stabilized random tilings are (with probability one) *locally indistinguishable*[8] from their images under symmetry transformations.

This is the main result of this section. Note that, also for tilings with a height representation, this is a much stronger statement than the demand $E \equiv 0$ on the phason strain, since different densities of symmetry related patches may be compatible with the same value for the phason strain.

6 Examples in two dimensions

6.1 The rhombus tiling – a domino tiling of Kasteleyn type with height representation

The rhombus random tiling [19, 14] is the ensemble of all coverings of the plane with 60°-rhombi. It is also called a lozenge tiling. It is a domino tiling on the triangular lattice, equivalent to the fully packed dimer model on the hexagonal lattice [39, 58]. We discuss it here since it is the prototype of a random tiling possessing a height representation, which allows us to demonstrate the equivalence of our approach to the conventional one, for this model. In the following, we focus on the symmetries of the tiling and give a simple

[8] An introduction to equivalence concepts of tilings is given in [5].

derivation of the entropy. In the appendix, we relate the elastic constant given by Henley [29, 30] to our result.

The symmetry of the random tiling ensemble which transforms rhombus tilings into other allowed ones is $D_6 = D_3 \times C_2$. For undecorated tiles, however, the inversion symmetry of the prototiles already enforces C_2 as (minimal) symmetry for any element of the tiling ensemble, thus $S_3 \simeq D_3$ remains as relevant geometric symmetry in the space of density parameters. There are no hidden symmetries in this case. Since all prototiles are related by rotation, for the point of maximal entropy we immediately conclude $\rho_1 = \rho_2 = \rho_3 = \frac{1}{3}$.

The filling constraint $\rho_1 + \rho_2 + \rho_3 = 1$ reduces the number of independent variables to two. As the symmetry acts irreducibly on the remaining two-dimensional subspace, the symmetry of the entropy function must belong to a two-dimensional irreducible representation of D_3. It is most convenient to represent the phase space as the set of points inside an equilateral triangle, see figure 2, this way obtaining a handy parametrization which we call its phase diagram. We choose its center as the origin and the vectors pointing

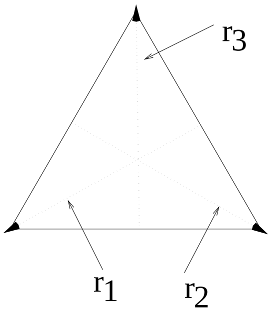

Figure 2: The phase space of the rhombus tiling is an equilateral triangle.

to the corners of the triangle as unit vectors of the different tile densities. The center corresponds to the point of maximal entropy, and each point $r = (r_1, r_2, r_3)$ corresponds to an ensemble with densities $\rho_i = r_i + \frac{1}{3}$. The symmetries of the entropy function are then reflected in the symmetries of the triangle. The point of maximum entropy is the only one with D_3 symmetry. Along lines with equal density of two different tiles there is reflection symmetry.

The grand-canonical potential per rhombus as a function of the different tile potentials $\mu_i = \log z_i$ (with $i = 1, 2, 3$) reads [58]

$$\begin{aligned} \phi(\mu_1, \mu_2, \mu_3) &= \frac{1}{8\pi^2} \int_0^{2\pi}\int_0^{2\pi} \log\det\lambda(\varphi_1, \varphi_2)\, d\varphi_1 d\varphi_2, \qquad (41) \\ &= \frac{1}{4\pi}\int_0^{2\pi} \log\left(\max\left\{z_1^2, z_2^2 + z_3^2 - 2z_2z_3\cos\varphi\right\}\right) d\varphi, \end{aligned}$$

where the determinant is given by

$$\det \lambda(\varphi_1, \varphi_2) = z_1^2 + z_2^2 + z_3^2 + 2z_1 z_2 \cos\varphi_1 + 2z_2 z_3 \cos\varphi_2 + 2z_3 z_1 \cos(\varphi_1 - \varphi_2).$$

This result was obtained by taking rhombohedral patches of increasing size, together with *periodic* boundary conditions. The result applies nevertheless to the corresponding limit with free boundary conditions, as can be seen as follows. The rhombus tiling can be regarded as a limiting case of the dart-rhombus tiling described below, where some chemical potentials are set to $-\infty$. This operation commutes with the *free* thermodynamic limit [46], yielding the same result as in (41).

We introduce the normalization constraint by setting

$$\tilde{\phi}(\mu_1, \mu_2) := \phi(\mu_1, \mu_2, 0). \tag{42}$$

The relation between $\tilde{\phi}$ and ϕ is given by

$$\tilde{\phi}\,(\mu_1 - \mu_3, \mu_2 - \mu_3) = \phi(\mu_1, \mu_2, \mu_3) - \mu_3, \tag{43}$$

$$\tilde{\rho}_1\,(\mu_1 - \mu_3, \mu_2 - \mu_3) = \rho_1(\mu_1, \mu_2, \mu_3), \qquad \tilde{\rho}_2\,(\mu_1 - \mu_3, \mu_2 - \mu_3) = \rho_2(\mu_1, \mu_2, \mu_3).$$

Let us determine the entropy curve as a function of the independent densities $\tilde{\rho}_1 = \rho_1$ and $\tilde{\rho}_2 = \rho_2$. From the normalized grand-canonical potential $\tilde{\phi}$ we obtain

$$z_1(\tilde{\rho}_1, \tilde{\rho}_2) = \frac{\sin \pi\tilde{\rho}_1}{\sin \pi(\tilde{\rho}_1 + \tilde{\rho}_2)}, \qquad z_2(\tilde{\rho}_1, \tilde{\rho}_2) = \frac{\sin \pi\tilde{\rho}_2}{\sin \pi(\tilde{\rho}_1 + \tilde{\rho}_2)}. \tag{44}$$

The expression for the entropy follows as

$$s(\tilde{\rho}_1, \tilde{\rho}_2) = -\int_0^{\tilde{\rho}_1} \log z_1(\tilde{\rho}, \tilde{\rho}_2) d\tilde{\rho} = -\int_0^{\tilde{\rho}_1} \log \frac{\sin \pi\tilde{\rho}}{\sin \pi(\tilde{\rho} + \tilde{\rho}_2)} d\tilde{\rho}. \tag{45}$$

At the point of maximum entropy we find

$$s_{\max} = \frac{1}{\pi} \sum_{k=1}^{\infty} \frac{\sin \frac{\pi}{3} k}{k^2} \approx 0.3230, \tag{46}$$

which is considerably smaller than the value $\frac{1}{\pi}\sum_{k=0}^{\infty} \frac{(-1)^k}{(2k+1)^2} \approx 0.583$ of the square lattice domino problem [38].

As the irreducible representation of the symmetry group is two-dimensional, we expect to have a single elastic constant. In fact, for the quadratic term in the entropy expansion we find

$$s_2(r, r) = -\frac{1}{2} \cdot \frac{\pi}{\sqrt{3}} \cdot 2(r_1^2 + r_1 r_2 + r_2^2). \tag{47}$$

On the other hand, the entropy function is defined on the subspace complementary to the vector $(1,1,1)^t$. This yields

$$I(r,r) = 2(r_1^2 + r_1 r_2 + r_2^2). \tag{48}$$

Thus we find an elastic constant of $\lambda = \frac{\pi}{\sqrt{3}}$. In the appendix we relate this constant to the constant given by Henley [29, 30] which was defined from the height representation of this model.

Note that there is a phase transition at points where two densities approach zero. In the above parametrization, this corresponds to the corners of the triangle. At these points, the covariance matrix shows a square-root singularity [14], indicating a phase transition of Kasteleyn type [48].

We give an expression of the entropy along a line of reflection symmetry: in the regime $\rho_1 = \rho_2$, we have

$$s(\rho_1) = \frac{2}{\pi} \int_0^{\pi\rho_1} \log 2\cos x dx. \tag{49}$$

This function is plotted in figure 3. The elastic constant is $\lambda = \frac{\pi}{\sqrt{3}}$.

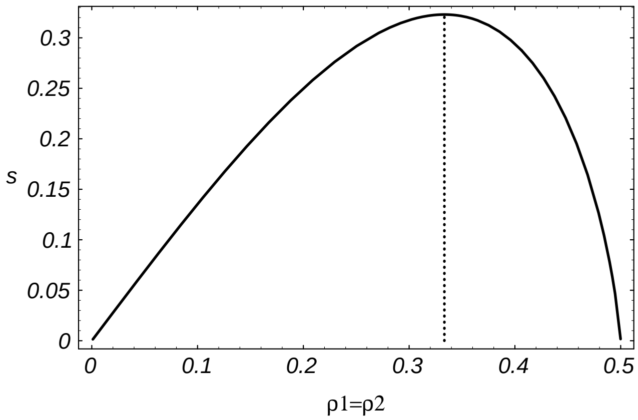

Figure 3: Entropy of the rhombus random tiling in the regime $\rho_1 = \rho_2$.

6.2 The dart-rhombus tiling – a domino tiling of Onsager type with hidden symmetry

We now present another random tiling of the domino class, but this time with two different types of prototiles [4]. It is therefore slightly more interesting than the model discussed above. The prototiles of the dart-rhombus random tiling are 60°-rhombi and darts made from two rhombus halfs, see figure 4. In addition to the usual face-to-face condition, we impose an alternation condition on the rhombi, such that neighbouring rhombi of equal orientation are excluded. Finally, to avoid pathologic lines of alternating darts, we demand that two neighbouring darts must not share a short edge. These tiling rules force the darts to arrange in closed lines, see figures 10 and 11. We thus deal with a *dilute loop model* of dart loops in a background of rhombi. For more on this picture, which we will not expand here, see [56]. The dense loop phase has the minimal total rhombus density $\rho = \frac{1}{3}$, see also figure 8.

This random tiling corresponds to the fully packed dimer system on one of the so-called Archimedian tilings (where all faces are regular polygons) [25]. Lattices and tilings of this type have already been described in detail by Kepler [41], but have since been rediscovered many times. In the context of statistical mechanics the graph of our model has also been called a Fisher lattice [57], its dual graph is named a Kagomé lattice. The

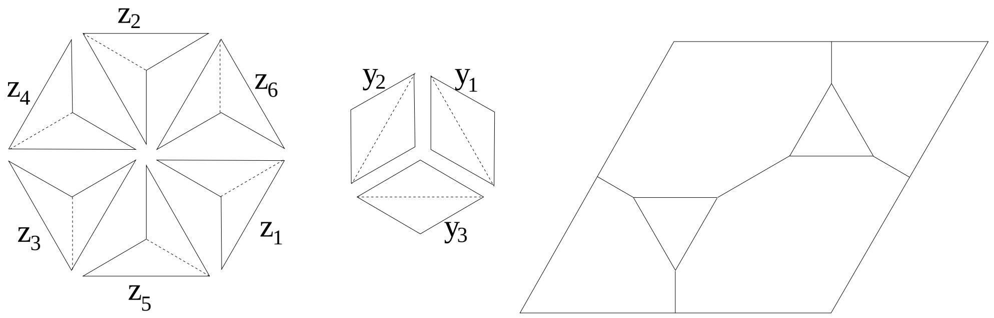

Figure 4: Prototiles of the dart-rhombus tiling and fundamental cell of the Fisher lattice.

first solution of the Fisher lattice dimer model was given by Fan and Wu [20] by realizing the correspondence to a soluble subcase of the the eight-vertex model [11], the so-called free-fermion case. A one-to-one mapping between the free-fermion case of the eight-vertex model [9] and the dart-rhombus tiling is obtained by a reformulation of the latter in terms of 'supertiles', see figure 5. Closed dart loops in the tiling correspond to closed edge loops on the square lattice.

Another interpretation exists as a model with domain walls where different walls can meet and annihilate [13], in generalization of the dimer system on the hexagonal lattice, which can also be interpreted as a domain-wall model. In our model, the domain walls correspond to the dart loops.

Let us denote the densities of rhombi by ρ_i $(i = 1, 2, 3)$ and the densities of darts by σ_i $(i = 1, \ldots, 6)$. We have several constraints on these macroscopic variables: in addition to the filling condition, the loop condition means that densities of opposite darts have to

[9] We follow the Baxter's convention here [11].

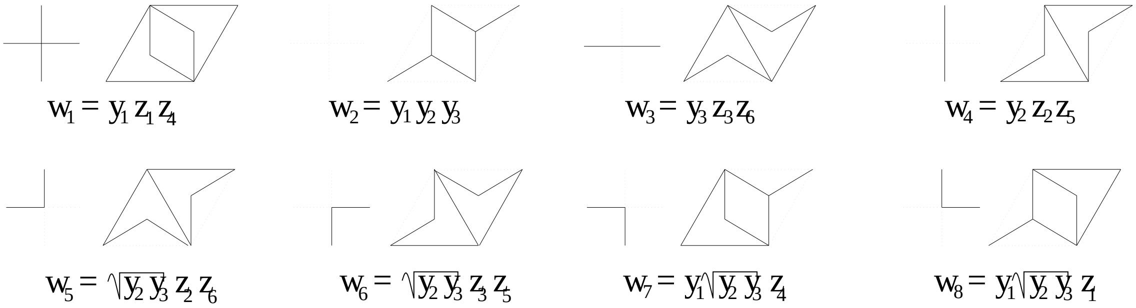

Figure 5: A mapping between the eight-vertex model and the dart-rhombus tiling via "super-tiles".

be the same,

$$\sigma_1 = \sigma_4, \qquad \sigma_2 = \sigma_5, \qquad \sigma_3 = \sigma_6. \tag{50}$$

Moreover, as each dart is accompanied by a rhombus of equal type, the remaining rhombi occur with equal frequency of each type due to the alternation condition,

$$\rho_1 - \sigma_1 = \rho_2 - \sigma_2 = \rho_3 - \sigma_3. \tag{51}$$

These constraints reduce the number of independent parameters to three.

The group of geometric symmetries of the tiling is D_3. But these are not the only symmetries of the model: there is a hidden symmetry which exchanges darts and rhombi. It is most easily described in the vertex model formulation where it corresponds to the exchange of free and occupied edges (spin reversal symmetry).

The full symmetry group of the dart-rhombus tiling turns out to be the *tetrahedral group* T_d. As the group action respects the density constraints and acts irreducible on the remaining subspace of independent density parameters, we can characterize the phase space of the dart-rhombus random tiling according to the three-dimensional irreducible representation of the tetrahedral group T_d. Each phase of the dart-rhombus tiling corresponds to a point inside the tetrahedron: we fix the tetrahedron center as the origin and choose an orthonormal basis of unit vectors pointing to edges along twofold axes, as is indicated in figure 6. In this way we obtain a parametrization in terms of reduced rhombi densities

$$r_i = \rho_i - \frac{1}{6} \qquad (i = 1, 2, 3). \tag{52}$$

The vectors pointing to the four corners of the tetrahedron are unit vectors for the reduced dart densities s_i and for the reduced total rhombi density r,

$$\begin{aligned} s_i &= 2\sigma_i - \tfrac{1}{6} \qquad (i = 1, 2, 3), \\ r &= r_1 + r_2 + r_3. \end{aligned} \tag{53}$$

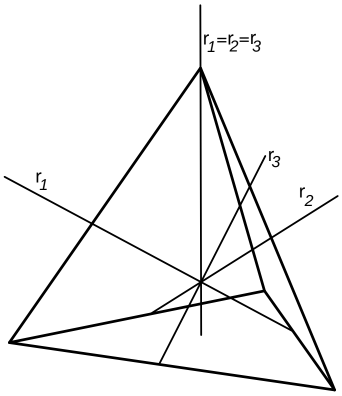

Figure 6: The phase space of the dart-rhombus tiling is a tetrahedron.

In this geometry, the dense loop phase is found on the triangle surface with minimal rhombus density $r = -\frac{1}{6}$. The other triangle surfaces which are obtained by the exchange symmetry are diluted phases where the darts arrange along directed lines due to exclusion of one dart orientation. On the other hand, the dense loop phase is an obvious decoration of the *rhombus tiling*, suggested by figure 8. We conclude that the surface phases are of Kasteleyn type with phase transitions at the corners of the tetrahedron.

The point of maximum entropy (the tetrahedron's centre) is fixed by symmetry to $\rho_i = \frac{1}{6}$, $\sigma_i = \frac{1}{12}$ where the darts and the rhombi occupy half of the tiling area each. The value at the entropy at its maximum

$$s_{\max} = \frac{1}{3} \log 2 \approx 0.231 \tag{54}$$

follows from a geometrical consideration: in the supertile formulation, building a rhombic patch by starting from a prescribed configuration on the left and on the upper boundary of a $\frac{\pi}{3}$ sector, there are in general two different possibilities to add a new tile. This results in an entropy of $\log 2$ per supertile because the choice of the boundary does not affect the entropy value. Observing that each supertile consists of 3 ordinary tiles by area, one obtains (54).

In general, phase transitions occur in regions where we have infinite dart lines which tend to minimize the enclosed area as in percolation, see figures 10 and 11. For a more concrete description, we introduce rhombus activities y_1, y_2, y_3, dart activities $z_1, \ldots, z_6$, and compute the grand-canonical potential per tile via Pfaffians, yielding [57]

$$\phi = \frac{1}{24\pi^2} \int_0^{2\pi} \int_0^{2\pi} \log \det \lambda(\varphi_1, \varphi_2) d\varphi_1 d\varphi_2, \tag{55}$$

where the determinant is given by

$$\begin{aligned}\det \lambda(\varphi_1, \varphi_2) &= y_1^2 z_1^2 z_4^2 + y_2^2 z_2^2 z_5^2 + y_3^2 z_3^2 z_6^2 + y_1^2 y_2^2 y_3^2 \\ &\quad +2y_1 y_2 (z_1 z_2 z_4 z_5 - y_3^2 z_3 z_6) \cos\varphi_1 \\ &\quad +2y_2 y_3 (z_2 z_3 z_5 z_6 - y_1^2 z_1 z_4) \cos(\varphi_1 - \varphi_2) \\ &\quad +2y_3 y_1 (z_1 z_3 z_4 z_6 - y_2^2 z_2 z_5) \cos\varphi_2 .\end{aligned}$$

This result was obtained by using *periodic* boundary conditions. It applies, however, in the case of nonzero activities, to the free case as well, since this has been shown by Ruelle [55] for the more general eight-vertex model. (Note that the Kasteleyn subclass has already been discussed above.)

Let us now proceed with the discussion of the critical behaviour as a function of the tile densities. It is of Onsager type in the generic case [20]. At points fulfilling the criticality condition

$$w_1 + w_2 + w_3 + w_4 = 2\max\{w_1, w_2, w_3, w_4\} \tag{56}$$

the grand-canonical potential is nonanalytic, resulting in a logarithmic divergence in the covariance matrix. The w_i $(i = 1, \ldots, 8)$ are the Boltzmann factors of the eight-vertex model whose relation to the tile activities is given in figure 5.

The entropy as a function of the rhombi densities indeed leads to a Hessian which is proportional to the identity. In the four-dimensional vector space of the reduced dart densities and the reduced total rhombus density, the entropy is defined on the hyperplane complementary to the vector $(1,1,1,1)^t$. This leads to

$$I(r,r) = 2(r_1^2 + r_2^2 + r_3^2), \qquad \lambda = 6. \tag{57}$$

Let us focus on the behaviour of the random tiling in the sixfold symmetric phase where each orientation of darts, respectively rhombi, occurs with the same frequency. The only free parameters are the total density ρ of the rhombi or the total density σ of the darts, each being equally distributed over the different orientations. The entropy curve as a function of the rhombus density ρ is plotted in figure 7. The maximum is already discussed above; the elastic constant in the sixfold phase is $\lambda = 6$. A phase transition of Onsager type occurs at $\rho = \frac{5}{6}$ with the usual logarithmic singularity in the isothermal compressibility. A phase transition of Kasteleyn type occurs at $\rho = 1$. The point $\rho = \frac{1}{3}$ is the point of maximal symmetry of the previously mentioned rhombus tiling (its maximum scaled by a factor of 3).

Below are four characteristic snapshots of tilings in the sixfold symmetric phase together with their diffraction patterns, taken at different rhombi densities [31]. The tilings are periodic in the vertical direction and periodic up to a cyclical shift in the horizontal direction. To obtain diffraction patterns, delta-scatterers were positioned in the middle of every prototile. Figures 8-11 show contour lines of the absolute value of the scatterer's Fourier transform, computed in arbitrary units.

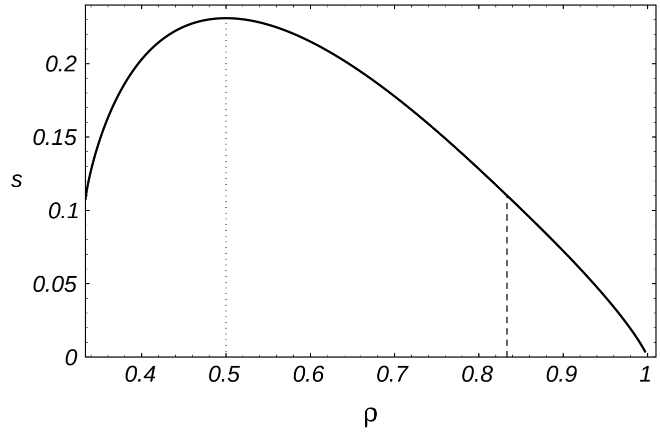

Figure 7: Entropy of the dart-rhombus random tiling in the sixfold symmetric phase as a function of the rhombus density ρ.

The phase transition (at rhombi density $\rho_c = \frac{5}{6}$) is directly visible in the tiling. Above the phase transition ($\rho > \rho_c$) we have just some small dart islands (figure 11) whereas below the phase transition ($\rho < \rho_c$) they form infinite lines as in percolation (figure 10). The phase transition is also visible in the diffraction pictures. Above the phase transition point, we have a small separated, sixfold symmetric background which gets connected below the phase transition.

At the entropy maximum (figure 9), the diffuse background has maximal intensity and is least structured whereas at minimal rhombus density (figure 8) it is still connected but laced up.

We mention that the height of the diffraction spots scales with the system size, as follows from our numerical analysis. The diffraction pattern in the thermodynamic limit consists of a point part (Bragg peaks) and an absolutely continous background [3]. Although this is not the generic result one expects for 2D random tilings, it is inevitable for this kind of crystallographic random tiling that lives on a lattice background.

6.3 Three-colourings of the square lattice – a monomino tiling violating the second random tiling hypothesis

The three-colouring model is the ensemble of tilings with three types of monominoes such that no two tiles of the same type are adjacent. Since the packing rule is of nearest-neighbour type, the restriction is hierarchical, and it is instructive to look at the one-dimensional model first. In one dimension, using the recursion method demonstrated above, the grand-canonical potential can be shown to be the logarithm of the positive

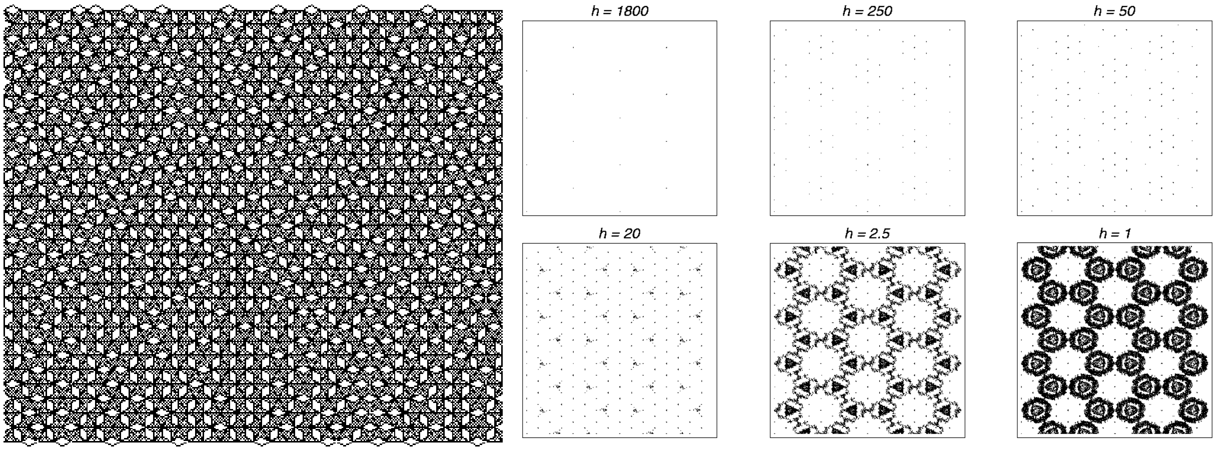

Figure 8: Minimal rhombi density ($\rho = 0.33$)

real root of the equation

$$x^3 - (z_1 z_2 + z_2 z_3 + z_3 z_1)x - 2 z_1 z_2 z_3 = 0, \tag{58}$$

the z_i being the activities of the different monominoes. By construction, the entropy of this ensemble is an upper bound for the entropy of its generalization to two dimensions.

The group S_3 of colour permutations is a symmetry for both models which also respects the filling constraint $\rho_1 + \rho_2 + \rho_3 = 1$. Consequently, the maximal entropy occurs at $\rho_1 = \rho_2 = \rho_3 = \frac{1}{3}$, and the thermodynamic functions are invariant under the two-dimensional irreducible action of the symmetry group in the subspace of independent densities. In particular, there is only one single elastic constant, which is $\lambda = 9$ for the one-dimensional model.

Bounds for the maximal entropy can be obtained as follows. The configurations with highest frequency of monominoes of type a are arrangements where all a's fill one sublattice. As the other vertices can independently be filled by monominoes of type b or c, we get a lower bound for the entropy: $s_{\max} \geq \log \sqrt{2}$. The one dimensional problem, at its point of maximal entropy, is a genuine Bernoulli type ensemble of entropy $\log 2$, so we found

$$0.3466 \approx \log \sqrt{2} \leq s_{\max} \leq \log 2 \approx 0.6931. \tag{59}$$

The given counting problem has first been solved by Baxter [8] using Bethe's Ansatz. Introducing chemical potentials μ_1, μ_2, μ_3 for the different monominoes, the grand-canonical potential reads [11]

$$\phi(\mu_1, \mu_2, \mu_3) = \log \frac{8(z_1 z_2 z_3)^{\frac{1}{3}}}{\sqrt{\frac{(u-w)^3}{v}} - \sqrt{\frac{(v-w)^3}{u}}}, \tag{60}$$

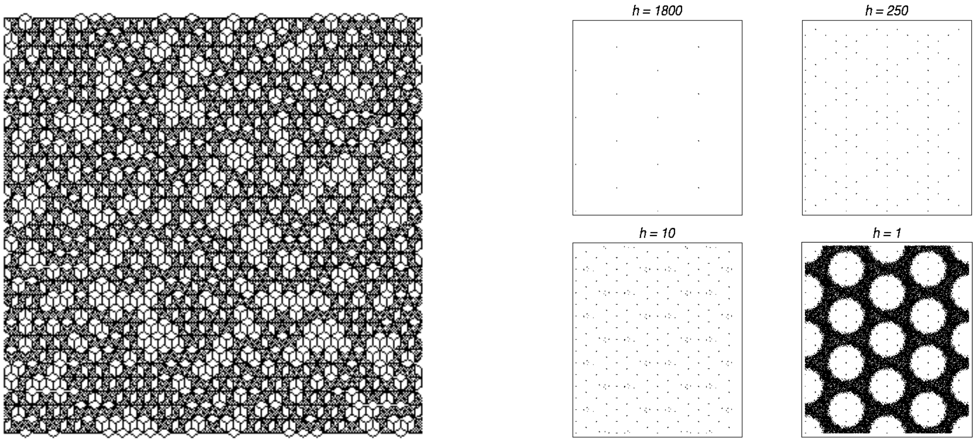

Figure 9: The entropy maximum ($\rho = 0.50$)

where u, v, w are the positive real solutions of

$$x(3B - x)^2 = 4, \qquad u > v \geq w, \tag{61}$$

where B is given by

$$B = \frac{z_1 z_2 + z_2 z_3 + z_1 z_3}{3(z_1 z_2 z_3)^{\frac{1}{3}}}. \tag{62}$$

It has to be stressed again that this solution was obtained by making use of *periodic* boundary conditions. The result agrees, on the other hand, with the corresponding free limit, as can be shown [56] by generalizing an argument of G. Kuperberg [42].

The value at the maximum entropy is

$$s_{\max} = \frac{3}{2} \log \frac{4}{3} \approx 0.4315, \tag{63}$$

which was already obtained before as the residual entropy of square ice [45].

It is instructive to analyse the entropy function along a line of reflection symmetry, see figure 12. Note that the entropy at its maximum is flat, indicating a vanishing second derivative, hence a phase transition at $s = s_{\max}$. The phase transition is of fluid-solid type: below the phase transition, monominoes arrange on the lattice homogeneously, whereas above the phase transition one sublattice is preferred in occupation [52]. The phase transition causes a square-root singularity in the covariance matrix [8].

In fact, explicit expressions for the entropy can be given in the two phases [56]. It turns out that both functions are analytic on the whole interval $0 \leq \rho < \frac{1}{2}$ and intersect smoothly at $\rho_1 = \frac{1}{3}$. They can therefore be polynomially approximated at the entropy maximum. The absolute values of the coefficients coincide up to fourth order; with

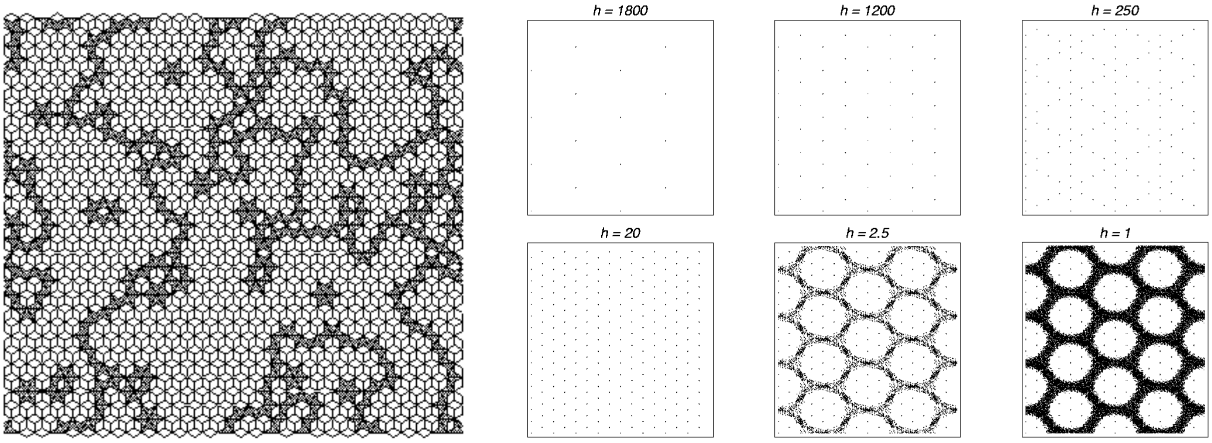

Figure 10: Below the phase transition ($\rho = 0.77$)

$r = \rho - \frac{1}{3}$, we find

$$s(r) = \frac{3}{2} \log \frac{4}{3} - \frac{1}{3!} \frac{9^2}{2} |r|^3 - \frac{1}{4!} \frac{9^3}{2} r^4 + \mathcal{O}(r^5). \tag{64}$$

We conclude that the square lattice three-colouring model violates the second random tiling hypothesis! This means that the usual reasoning about elastic theory [30] is not applicable here.

It would be interesting to compare this result with an expansion of the entropy in terms of variables taken from the height representation of this model [16].

6.4 Hard hexagons – a monomino tiling with unexpected entropy

Our last example belongs to a tiling class with two kinds of monominoes which we call particles and holes together with nearest neighbour exclusion for the particles. Its one-dimensional version has already been discussed above. The two-dimensional generalizations to the square lattice and to the hexagonal lattice correspond to the ensembles of *hard squares* [10, 21] and *hard hexagons* [9, 11]. Both models show a kind of fluid-solid phase transition: the low density phase is homogeneous, each sublattice has the same particle density, whereas at high density one sublattice is preferred in occupation. There is no obvious symmetry in these models, and therefore no preferred point in the phase space where the entropy maximum should be located.

It is interesting to mention that the three-colouring model discussed above was interpreted as an 'approximating' hard squares model, with two types of holes [8, 52]. As the hard squares model itself has escaped exact solution so far, we concentrate on the hard hexagon model in the following. The solution of this model was given by Baxter

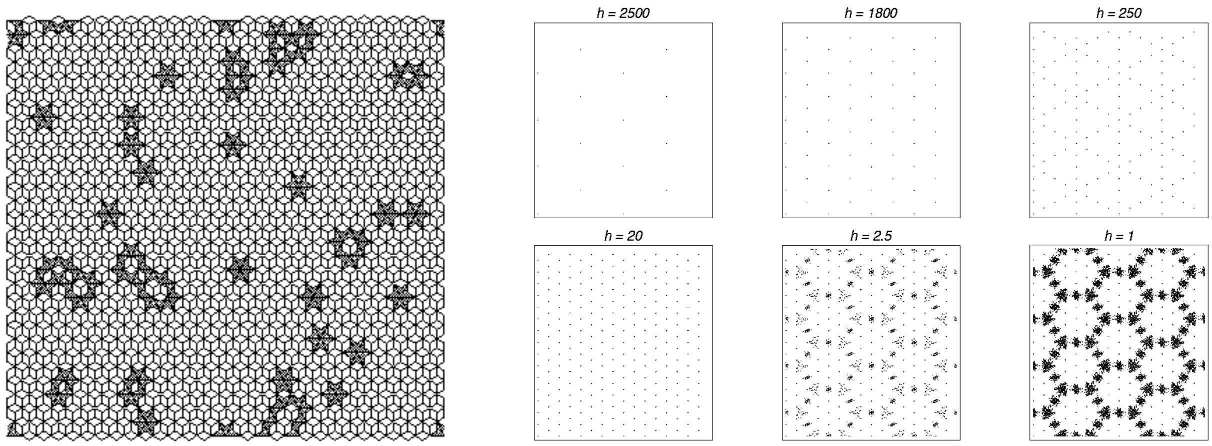

Figure 11: Above the phase transition ($\rho = 0.90$)

[9, 11]. This result is again obtained from *periodic* boundary conditions. It is easy to see, however, that it coincides with the result for the corresponding free boundary conditions, as each free rectangular patch can be transformed into a periodic one by adding a row of holes.

A phase transition occurs at $\rho_c = \frac{1}{\tau\sqrt{5}} \approx 0.2764$ (the maximal density being normalized to $\frac{1}{3}$) with a critical exponent $\alpha = \frac{1}{3}$ in the covariance matrix. The entropy is a concave function with a quadratic maximum

$$s_{\max} \approx 0.333243 \quad \text{at} \quad \rho \approx 0.162433. \tag{65}$$

Note that the maximum occurs nearly at the point where the hexagons occupy half of the lattice area. The small deviation of the entropy from $\frac{1}{3}$ lead to an incorrect prediction [10] in 1978. The elastic constant turns out to be $\lambda \approx 24.0807$.

Joyce [36] used the theory of modular functions to write the particle activity z as an *algebraic* function of the mean density ρ. Applying Joyce's results, one can in fact find closed expressions for $s_{\max}, \rho$ and λ. As these are quite complicated, we omit them here [56].

7 Concluding remarks

We have shown, both conceptually and by a number of examples, that the densities of tiles in random tiling ensembles provide natural parameters to investigate the phase diagram of such models. This is then independent of the existence of a height representation, but fully consistent with it if it happens to exist.

[10] For a short history of the model, see chapter 14.1 of Baxter's book [11].

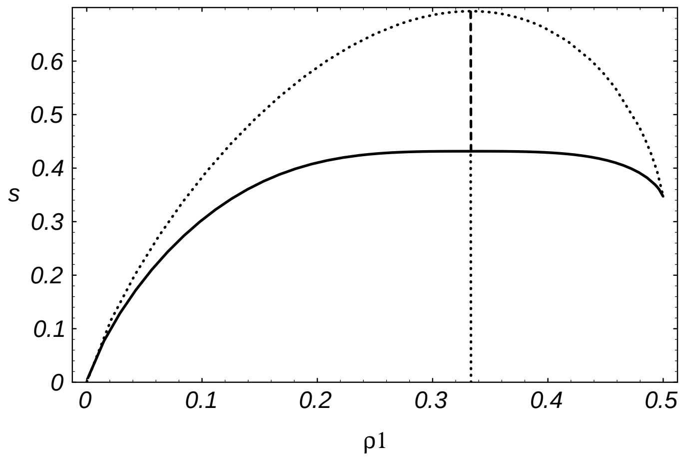

Figure 12: Entropy of the three-colouring model along a line of reflection symmetry ($\rho_2 = \rho_3$) as a function of ρ_1 (heavy curve). The dotted curve represents the system with exclusion restricted to one dimension.

Whereas the re-interpretation of exactly solvable models directly leads to a number of random tilings with analytic expressions for the entropy function, it is much more difficult to extract information about diffraction properties via Fourier transforms because this also requires the knowledge of the autocorrelation. For simple models such as the domino tiling and the rhombus tiling, it is possible [3] to compute the diffraction Bragg part explicitly and also the behaviour of the diffuse background in the thermodynamic limit.

The next step in the analysis of random tilings is certainly the application of the concept developed so far to quasicrystalline random tilings. Although there are recent exact results on rectangle-triangle tilings [22, 37], the interpretation of some of the results, for example the shape of the entropy curve in the solvable regime, is subject to controversial discussion. It may turn out that the framework of statistical mechanics proposed here gains additional insight into the phase space of the tilings.

Acknowledgements

It is our pleasure to thank Paul Pearce for several useful hints and some help with the body of known results and Elliott Lieb for a number of clarifying discussions. We thank Chris Henley for numerous valuable comments on the manuscript. Financial support from the German Science Foundation (DFG) is gratefully acknowledged.

Appendix: Height representation of the rhombus tiling

Here, we briefly describe the connection between our description of the rhombus tiling to the description by Henley [29, 30]. In particular, we show the connection between the elastic constants defined by both approaches.

As was first pointed out in [14], each configuration of the rhombus tiling can be obtained by projecting a roof-type surface in the cubic lattice to the diagonal hyperplane. In this way, the rhombus tiling possesses a natural height representation. As the average slope of this surface determines the average densities of the different tiles and vice versa, we can parametrize the ensemble alternatively by some slope variables.

Let us describe this more formally. Our vector space is R^3 with the standard scalar product $< \cdot, \cdot >$. The diagonal hyperplane in R^3 can be described by its normal vector $e^{\perp} = \frac{1}{\sqrt{3}}(1,1,1)^t$. We call the space spanned by $e^{\perp}$ *perp(endicular) space* $V^{\perp}$ and the complementary hyperplane *physical space* $V^{||}$. Let us denote the projections of vectors $x \in R^3$ to these subspaces by $x^{\perp}$ resp. $x^{||}$. The *perp strain tensor* E is a linear map

$$E : V^{||} \to V^{\perp}. \tag{66}$$

E defines a hyperplane in R^3. By definition, $E \equiv 0$ corresponds to $V^{||}$. We define matrix elements E_1, E_2 of E:

$$E_1 e_1^{\perp} = E e_1^{||}, \qquad E_2 e_2^{\perp} = E e_2^{||}. \tag{67}$$

A normal vector to this hyperplane is given by $(1 - E_1, 1 - E_2, 1 + E_1 + E_2)^t$.

We can easily relate the average slope of a surface parametrized by $E = (E_1, E_2)$ to the mean densities of the projected tiles:

$$\rho_1 = \frac{1}{3}(1 - E_1), \qquad \rho_2 = \frac{1}{3}(1 - E_2). \tag{68}$$

The quadratic form (47) can (with $r = \rho - \frac{1}{3}$) be rewritten in the form

$$s_2(E, E) = -\frac{1}{2} \cdot \frac{2}{\sqrt{3}} \cdot \frac{\pi}{9} \cdot (E_1^2 + E_1 E_2 + E_2^2). \tag{69}$$

This is the expression given by Henley [29, 30] up to a constant of $\frac{2}{\sqrt{3}}$ which arises from different normalizations of unit vectors in physical and perp space in his setup.

References

[1] M. Abramowitz and I. Stegun, *Handbook of mathematical functions*, Dover publications, New York (1972).

[2] M. Baake, V. Elser and U. Grimm, *On the entropy of square-free words*, Mathl. Comput. Modelling **26** (1997) 13-26.

[3] M. Baake and M. Höffe, *Comments on the diffraction of random tilings* (in preparation).

[4] M. Baake, J. Hermisson, M. Höffe and C. Richard, *Random tilings and dimer models*, Proc. Int. Conf. Quasicrystals 6 (Tokyo), ed S. Takeuchi and T. Fujiwara, World Scientific, Singapore (1998) p. 128-131.

[5] M. Baake and M. Schlottmann, *Geometric aspects of tilings and equivalence concepts*, Proc. Int. Conf. Quasicrystals 5 (Avignon), editors C.Janot and R. Mosseri, World Scientific, Singapore (1995) p. 15-21.

[6] R. Balian, *From microphysics to macrophysics*, vol. 1, Springer, Berlin (1991).

[7] H. Bauer, *Wahrscheinlichkeitstheorie*, de Gruyter, Berlin (1991).

[8] R.J. Baxter, *Three-colourings of the square lattice: a hard squares model*, J. Math. Phys. **11** (1970) 3116-3124.

[9] R.J. Baxter, *Hard hexagons: exact solution*, J. Phys. **A 13** (1980) L61-L70.

[10] R.J. Baxter, I. G. Enting and S. K. Tsang, *Hard-square lattice gas*, J. Stat. Phys. **22** (1980) 465-489.

[11] R.J. Baxter, *Exactly Solved Models in Statistical Mechanics*, Academic Press, London (1982).

[12] S.I. Ben-Abraham, *Defective vertex configurations in quasicrystalline structures*, Int. Journ. Mod. Phys. **B7** (1993) 1415-1425.

[13] S. M. Bhattacharjee, *Crossover in an exactly solvable dimer model of domain walls with dislocations*, Phys. Rev. Lett. **53** (1984) 1161-1163.

[14] H.W.J. Blöte and H.J. Hilhorst, *Roughening transitions and the zero-temperature triangular Ising antiferromagnet* J. Phys. **A15** (1982) L631-L637.

[15] M. de Boissieu, P. Stephens, M. Boudard, C. Janot, D.L. Chapman and M. Audier, *Evidence for random disorder in the perfect icosahedral phase of AlPdMn*, Proc. Int. Conf. Aper. Cryst. (1994), World Scientific, Singapore, p. 535-540.

[16] J. K. Burton and C. L. Henley *Simulations of a constrained antiferromagnetic Potts model* J. Phys. A **30** (1997) 8385-8413.

[17] G. Coddens, *Models for assisted phason hopping and phason elasticity in icosahedral quasicrystals*, Int. Journ. Mod. Phys. **B 11** (1997) 1679-1716.

[18] V. Elser, *Comments on "Quasicrystals: a new class of ordered structures"*, Phys. Rev. Lett. **54** (1985) 1730-1730,
Indexing problems in quasicrystals diffraction, Phys. Rev. **B32** (1985) 4892-4898.

[19] V. Elser, *Solution of the dimer problem on a hexagonal lattice with boundary*, J. Phys. A **17** (1984) 1509-1513.

[20] C. Fan and F.Y. Wu, *General model of phase transitions*, Phys. Rev. **B2** (1970) 723-733.

[21] D.S. Gaunt and M.E. Fisher, *Hard-sphere lattice gases. I. Plane-square lattice gas*, J. Chem. Phys. **43** (1965) 2840-2489.

[22] L. de Gier and B. Nienhuis, *Exact solution of an octagonal tiling model*, Phys. Rev. Lett. **76** (1996) 2918-2921,

J. de Gier and B. Nienhuis, *The exact solution of an octagonal rectangle-triangle random tiling, J. Stat. Phys.* **87** (1997) 415-437,

J. de Gier and B. Nienhuis, *Bethe Ansatz solution of a decagonal rectangle triangle random tiling*, J. Phys. A **31** (1998) 2141-2154.

[23] S.W. Golomb, *Polyominoes: puzzles, patterns, problems, and packings*, 2nd. edition, Princeton University Press, Princeton, New Jersey (1994).

[24] D. Grensing and G. Grensing, *Boundary effects in the dimer problem on a non-Bravais lattice*, J. Math. Phys. **24** (1983) 620-630,

D. Grensing, I. Carlsen and H.Chr. Zapp, *Some exact results for the dimer problem on plane lattices with non-standard boundaries*, Phil. Mag. A **41** (1980) 777-781.

[25] B. Grünbaum and G. C. Shephard, *Tilings and patterns*, W. H. Freeman and Company, New York (1987).

[26] P. Guyot, P. Kramer and M. de Boissieu, *Quasicrystals*, Rep. Prog. Phys. **54** (1991) 1373-1425.

[27] M. Hamermesh, *Group theory and its application to physical problems*, Dover publications, New York (1962).

[28] O.J. Heilmann and E.H. Lieb, *Monomers and dimers*, Phys. Rev. Lett. **24** (1970) 1412-1414,

O.J. Heilmann and E.H. Lieb, *Theory of monomer-dimer systems*, Comm. Math. Phys. **25** (1972) 190-232.

[29] C.L. Henley, *Random tilings with quasicrystal order: transfer-matrix approach*, J. Phys. **A 21** (1988) 1649-1677.

[30] C.L. Henley, *Random Tiling Models*, in *Quasicrystals: The State of the Art* (1991), ed. D.P. DiVincenzo and P. Steinhardt, 429-524.

[31] M. Höffe, *Zufallsparkettierungen und Dimermodelle*, Diplomarbeit, Universität Tübingen (1997).

[32] C. Janot, *Quasicrystals – a primer*, 2nd. ed., Clarendon Press, Oxford (1994).

[33] D. Joseph and V. Elser, *A model of quasicrystal growth*, Phys. Rev. Lett. **79** (1997) 1066-1069.

[34] D. Joseph and M. Baake, *Boundary conditions, entropy and the signature of random tilings*, J. Phys. **A 29** (1996) 6709-6716.

[35] D. Joseph, S. Ritsch and C. Beeli, *Distinguishing quasiperiodic from random order in high-resolution TEM images*, Phys. Rev. **B 55** (1997) 8175-8183.

[36] G.S. Joyce, *On the hard-hexagon model and the theory of modular functions*, Phil. Trans. R. Soc. Lond. A **325** (1988) 643-702.

[37] P.A. Kalugin, *The square-triangle random tiling model in the thermodynamic limit*, J. Phys. **A 27** (1994) 3599-3614,

P.A. Kalugin, *Low-lying excitations in the square-triangle random tiling model*, J. Phys. **A 30** (1997) 7077-7087.

[38] P.W. Kasteleyn, *The statistics of dimers on a lattice*, Physica **27** (1961) 1209-1225.

[39] P.W. Kasteleyn, *Dimer statistics and phase transitions*, J. Math. Phys. **4** (1963) 287-293.

[40] R. Kenyon, *Local statistics of lattice dimers*, Ann. Inst. H. Poincaré, Probabilités, **33** (1997) 591-618.

[41] I. Keppler [J. Kepler] *Harmonice Mundi*, Lincii (1619).

[42] G. Kuperberg, private communication.

[43] J.C. Lagarias and D.S. Romano, *A polyomino tiling problem of Thurston and its configurational entropy*, J. Comb. Theory **A 63** (1993) 338-358.

[44] W. Li, H. Park and M. Widom, *Phase diagram of a random tiling quasicrystal*, J. Stat. Phys. **66** (1992) 1-69.

[45] E.H. Lieb, *Residual entropy of square ice*, Phys. Rev. **162** (1967) 162-172.

[46] E.H. Lieb and F.Y. Wu, *Two-dimensional ferroelectric models*, in *Phase Transitions and Critical Phenomena*, Vol. 1, (ed. C.Domb and J.L.Lebowitz), Academic Press, London (1972), p.331-490.

[47] T.C. Lubensky, in *Aperiodic Crystals I: Introduction to quasicrystals*, ed. M. V. Jaric, Academic Press (1988).

[48] J.F. Nagle, *Dimer Models on Anisotropic Lattices*, in *Phase Transitions and Critical Phenomena*, Vol. 13, (ed. C.Domb and J.L.Lebowitz), Academic Press, London (1989), p.236-297.

[49] H.-U. Nissen and C. Beeli, *Electron microscopy of quasicrystals and the validity of the tiling approach*, Int. J. Mod. Phys. **B7** (1993) 1387-1413.

[50] G. van Ophuysen, M. Weber and L. Danzer, *Strictly local growth of Penrose patterns*, J. Phys. **A 28** (1995) 281-290.

[51] R.K. Pathria, *Statistical mechanics*, Pergamon press, Oxford (1977).

[52] P. A. Pearce and K. A. Seaton, *Exact solution of cyclic solid–on–solid lattice models*, Ann. Phys. **193** (1989) 326-366.

[53] K. Petersen, *Ergodic theory*, Cambridge University Press, Cambridge (1983).

[54] J. Propp, *Boundary-dependent local behaviour for 2-D dimer models*, Int. J. Mod. Phys. **B 11** (1997) 183-187.

[55] D. Ruelle, *Statistical Mechanics: Rigorous results*, W.A. Benjamin, London (1969).

[56] C. Richard, *Entropie in periodischen und nichtperiodischen Festkörpern*, Dissertation, Universität Tübingen, in preparation.

[57] C.J. Thompson, *Mathematical Statistical Mechanics*, Princeton University Press, Princeton, New Jersey (1972).

[58] F.Y. Wu, *Remarks on the modified Potassium Dihydrogen Phosphate Model of a Ferroelectric*, Phys. Rev. **168** (1968) 539-543.

[59] F.Y. Wu, *Eight-vertex model on the honeycomb lattice*, J. Math. Phys. **15** (1974) 678-681.